Electronic Supplementary Material (ESI) for Physical Chemistry Chemical Physics.

Supporting Information

Neat ionic liquids versus ionic liquid mixtures: combination of experimental data and molecular simulation

Andreia S. L. Gouveia,[a] *Carlos E. S. Bernardes,*[a] *Elena I. Lozinskaya,*[c] *Alexander S. Shaplov,*[d] *José N. Canongia Lopes*[*a] *and Isabel M. Marrucho*[*ab]

[a] Centro de Química Estrutural, Departamento de Engenharia Química, Instituto Superior Técnico, Universidade de Lisboa, Avenida Rovisco Pais, 1049-001 Lisboa, Portugal.

[b] Instituto de Tecnologia Química e Biológica António Xavier, Universidade Nova de Lisboa, Av. da República, 2780-157 Oeiras, Portugal.

[c] A.N. Nesmeyanov Institute of Organoelement Compounds Russian academy of sciences (INEOS RAS), Vavilov St., 28, 119991 Moscow, Russia

[d] Luxembourg Institute of Science and Technology (LIST), 5 avenue des Hauts-Fourneaux, L-4362, Esch-sur-Alzette, Luxembourg

* Corresponding authors:

E-mails: jnlopes@tecnico.ulisboa.pt; isabel.marrucho@tecnico.ulisboa.pt

Samples

The 1-ethyl-3-methylimidazolium thiocyanate ([C_2mim][SCN]), > 98 wt%, IoLiTec) and 1-ethyl-3-methylimidazolium trifluoromethanesulfonate ([C_2mim][CF_3SO_3], ≥ 98 wt%, Aldrich), 1-ethyl-3-methylimidazolium bis(trifluoromethylsulfonyl)imide ([C_2mim][NTf_2]), > 99 wt%, Solvionic), 1-ethyl-3-methylimidazolium dicyanamide ([C_2mim][$N(CN)_2$]), > 98 wt%, IoLiTec) were obtained from the specified suppliers. The 1-ethyl-3-methylimidazolium 2,2,2-trifluoromethylsulfonyl-N-cyanoamide ([C_2mim][TFSAM]) IL (98.5–99.0 wt% pure) was synthesized according to a described procedure[1] as referred in our previous works.[2, 3]

The equimolar [C_2mim][SCN]$_{0.5}$[CF_3SO_3]$_{0.5}$ and [C_2mim][$N(CN)_2$]$_{0.5}$[NTf_2]$_{0.5}$ mixtures were prepared using an analytical high precision balance with an uncertainty of ± 10^{-5} g by syringing known masses of the neat IL components into a glass vial. Good mixing was assured by magnetic stirring for 30 min at room temperature under inert atmosphere.

In order to reduce the content of water and other volatile substances, all IL samples were dried at approximately 1 Pa and 318 K for at least 4 days and their H_2O content was determined by Karl Fischer titration using an 831 KF Coulometer (Metrohm).

Density and Viscosity Determination

The density and viscosity measurements of the studied IL samples were performed in the temperature range between 293.15 and 353.15 K at atmospheric pressure using an SVM 3000 Anton Paar rotational Stabinger viscometer-densimeter, where the standard uncertainty for the temperature is 0.02 K. The repeatability of density and dynamic viscosity of this equipment is 0.0005 g cm^{-3} and 0.35%, respectively. The reported results are average values since triplicates of each sample were performed to ensure accuracy.

The highest absolute standard uncertainty registered for the density and dynamic viscosity measurements was $3\cdot10^{-3}$ and 0.03, respectively.

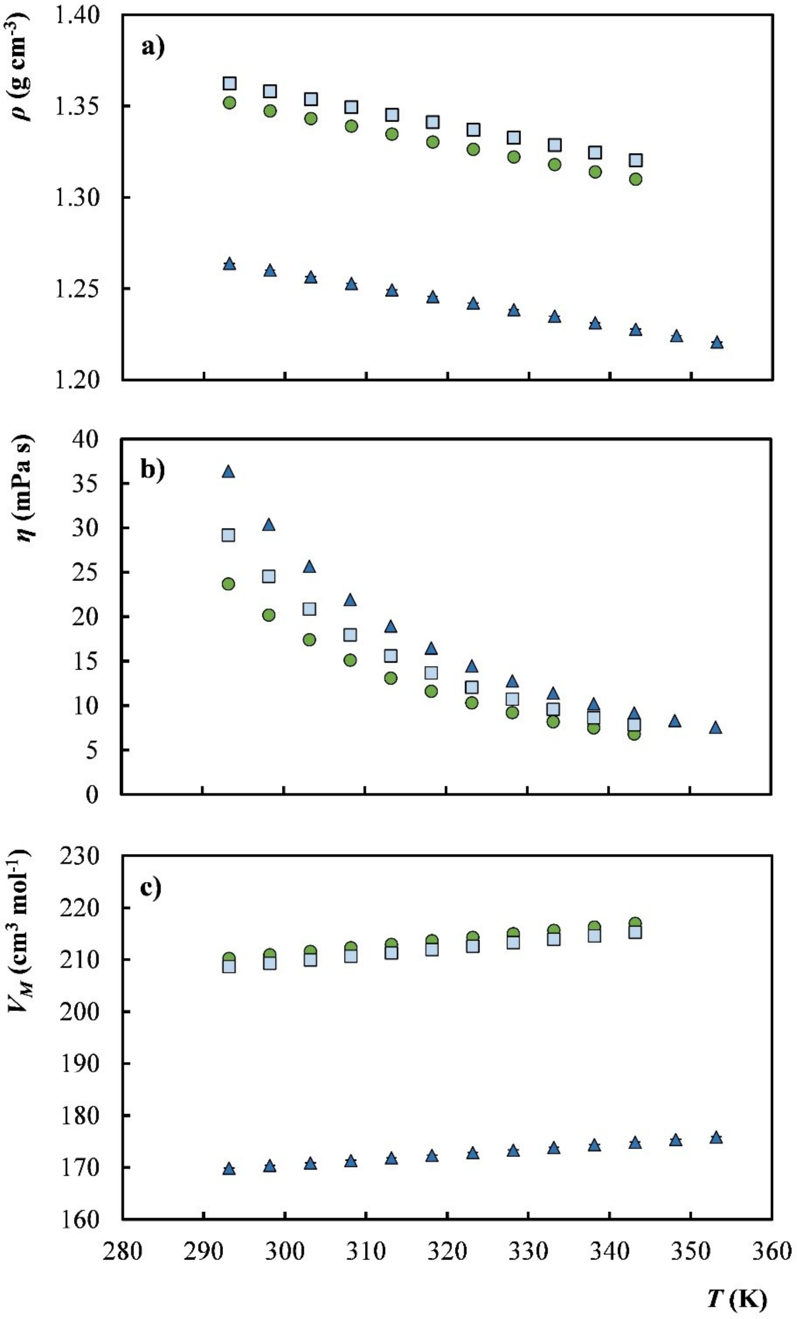

Figure 1. a) Density, **b)** dynamic viscosity and **c)** calculated molar volume values as a function of temperature: ●, $[C_2mim][TFSAM]$; ▲, $[C_2mim][SCN]_{0.5}[CF_3SO_3]_{0.5}$; ■, $[C_2mim][N(CN)_2]_{0.5}[NTf_2]_{0.5}$. Absolute standard uncertainties *u* are $u(\rho) = 0.003$; $u(\eta) = 0.03$; $u(Vm) = 0.05$. The errors bars marked in all graphs are smaller than the symbols used to represent the experimental data.

Table S1. Experimental densities, ρ (g cm^{-3}), viscosities, η (mPa s), and calculated molar volumes, V_M (cm^3 mol^{-1}), of neat [C$_2$mim][TFSAM] and studied IL-IL mixtures.[*]

	ρ (g cm^{-3})			**η (mPa s)**			**V_M (cm^3 mol^{-1})**		
T(K)	**[C$_2$mim][TFSAM]**[a]	**[C$_2$mim][SCN][CF$_3$SO$_3$]**	**[C$_2$mim][N(CN)$_2$][NTf$_2$]**[b]	**[C$_2$mim][TFSAM]**[a]	**[C$_2$mim][SCN][CF$_3$SO$_3$]**	**[C$_2$mim][N(CN)$_2$][NTf$_2$]**[b]	**[C$_2$mim][TFSAM]**[a]	**[C$_2$mim][SCN][CF$_3$SO$_3$]**	**[C$_2$mim][N(CN)$_2$][NTf$_2$]**[b]
293.15	1.352	1.264	1.362	23.7	36.4	29.2	210.3	169.9	208.7
298.15	1.347	1.260	1.358	20.2	30.4	24.5	211.0	170.4	209.3
303.15	1.343	1.256	1.354	17.4	25.7	20.9	211.6	170.9	210.0
308.15	1.339	1.253	1.349	15.1	21.9	18.0	212.3	171.4	210.7
313.15	1.335	1.249	1.345	13.1	18.9	15.6	213.0	171.9	211.3
318.15	1.330	1.246	1.341	11.6	16.5	13.7	213.7	172.4	212.0
323.15	1.326	1.242	1.337	10.3	14.5	12.1	214.3	172.9	212.6
328.15	1.322	1.238	1.333	9.2	12.8	10.7	215.0	173.4	213.3
333.15	1.318	1.235	1.329	8.2	11.4	9.6	215.7	173.9	214.0
338.15	1.314	1.231	1.325	7.5	10.2	8.6	216.3	174.4	214.6
343.15	1.310	1.228	1.320	6.8	9.2	7.8	217.0	174.9	215.3
348.15	-	1.224	-	-	8.3	-	-	175.4	-
353.15	-	1.221	-	-	7.6	-	-	175.9	-

[*] Absolute standard uncertainties u are $u(\rho) = 0.003$; $u(\eta) = 0.03$; $u(V_M) = 0.05$.
[a] The density, viscosity and molar volume values of [C$_2$mim][TFSAM] were taken from Gouveia *et al.*[3]
[b] The density, viscosity and molar volume values of [C$_2$mim][N(CN)$_2$][NTf$_2$] mixture were taken from Tomé *et al.*[4]

The density data was fitted as a function of temperature, T (K), using Eq. 1:

$$\rho = a + b\,(T) \qquad (1)$$

The adjustable parameters, a and b, as well as the correlation coefficient, R^2, are listed in Table S2. Looking at R^2 values, it can be concluded that the use of the linear function adequately described the measured density data, for the temperature range studied.

Table S2. Fitted parameters, a and b, of the linear expression given by Eq. 1 as well as the correlation coefficients, R^2.[a]

IL Sample	a ($g \cdot cm^{-3}$)	$b \times 10^4$ ($g \cdot cm^{-3} K^{-1}$)	R^2
$[C_2mim][TFSAM]$	1.597	-8.37	0.9999
$[C_2mim][SCN][CF_3SO_3]$	1.474	-7.17	1.0000
$[C_2mim][N(CN)_2][NTf_2]$	1.608	-8.38	0.9999

[a] Standard uncertainties u are $u(a) = 0.001$, $u(b) = 3 \cdot 10^{-6}$.

The experimental viscosity values were fitted as a function of temperature, using the Vogel−Fulcher−Tammann (VFT) model described in Eq. 2:

$$\ln \eta = A_\eta + \frac{B_\eta}{(T - C_\eta)} \qquad (2)$$

where η is the viscosity in mPa s, T is the temperature in K, and $A\eta$, $B\eta$, and $C\eta$ are adjustable parameters. The adjustable parameters, which were determined from the fitting of the experimental data, are listed in Table S3, along with the energy barrier of a fluid to shear stress, E, (kJ mol^{-1}) derived at 298.15 K and the absolute average relative deviation (ARD) for both mixtures and neat $[C_2mim][TFSAM]$ IL.

The energy barrier was determined based on the viscosity dependence with temperature using Eq. 3, as follows:[5]

$$E = R.\frac{\partial(\ln \eta)}{\partial\left(\frac{1}{T}\right)} = R.\left(\frac{B_\eta}{\left(\frac{C_\eta^2}{T^2} - \frac{2C_\eta}{T} + 1\right)}\right) \tag{3}$$

where η is the viscosity, T is the temperature, $B\eta$ and $C\eta$ are the adjustable parameters obtained from Eq. 2, and R is the universal gas constant.

Table S3. Adjustable parameters, *a* and *b*, of the linear expression used to fit the experimental density as a function of temperature as well as the correlation coefficient, R^2.

IL Sample	**Parameters**			**ARD (%)**	**R^2**	**$E_{298.15K}$**
	A_η (mPa s)	**B_η (K)**	**C_η (K)**			**(kJ mol^{-1})**
[C_2mim][TFSAM]	-1.82	743.55	144.14	0.06	1.000	20.9
[C_2mim][SCN][CF_3SO_3]	-1.72	760.25	150.04	0.01	1.000	22.3
[C_2mim][$N(CN)_2$][NTf_2]	-1.66	711.13	151.82	0.02	1.000	21.9

Although the *E* values are all very similar, neat [C_2mim][TFSAM] IL presents the lowest *E* value, which means that the ions have less difficulty to move past each other in this case.

Table S4. Excess Molar Volumes, V^E ($cm^3\ mol^{-1}$), and excess logarithm viscosities, $(\ln \eta)^E$ (mPa s), of $[C_2mim][SCN][CF_3SO_3]$ and $[C_2mim][N(CN)_2][NTf_2]$ binary mixtures

	V^E ($cm^3\ mol^{-1}$)		**$(\ln \eta)^E$ (mPa s)**	
T(K)	**$[C_2mim][SCN][CF_3SO_3]$**	**$[C_2mim][N(CN)_2][NTf_2]$**	**$[C_2mim][SCN][CF_3SO_3]$**	**$[C_2mim][N(CN)_2][NTf_2]$**
293.15	0.340	0.166	-0.020	0.097
298.15	0.350	0.186	-0.019	0.093
303.15	0.358	0.134	-0.018	0.092
308.15	0.354	0.154	-0.017	0.088
313.15	0.353	0.159	-0.016	0.085
318.15	0.349	0.148	-0.015	0.081
323.15	0.350	0.077	-0.014	0.078
328.15	0.353	0.082	-0.013	0.074
333.15	0.347	0.159	-0.012	0.071
338.15	0.350	0.147	-0.011	0.066
343.15	0.341	0.152	-0.011	0.063
$u(V^E)$; $u(\Delta\eta)$ [a]	0.016	0.059	0.012	0.008

used in this work.

[a] $u(V^E)$ ($cm^{-3}\ mol^{-1}$) and $u(\eta^E)$ (mPa s) are the standard uncertainties u.

Differential Scanning Calorimetry (DSC)

Thermal properties of ILs and IL-IL mixtures were studied by differential scanning calorimetry (DSC) using Q100 differential calorimeter (TA Instruments) in the temperature range from –80 to 80 °C at a heating rate of 2 °C min^{-1}. Prior to measurements, the calorimeter was calibrated using the indium calibration standard (Mettler-Toledo, purity > 99.999 %). All samples were weighed (sample weight ~9-20 mg) with the precision of ± 0.0001 g and hermetically sealed in aluminum pans inside an argon-filled glovebox (MBRAUN MB-Labstar, H_2O and O_2 content <0.5 ppm). Commonly two cycles at 2 °C min^{-1} from 25 °C to -80 and from -80 to 80°C were performed, where only the second cycle was further evaluated as the first one was used to eliminate the thermal history of the sample.

Due to high viscosity of ILs an extra accurate measurement of their thermal properties is required. Thus, a very low heating rate of 2 °C min^{-1} was chosen.[6, 7] For [C$_2$mim][TFSAM],[1] [C$_2$mim][N(CN)$_2$],[8] [C$_2$mim][NTF$_2$][9] and [C$_2$mim][CF$_3$SO$_3$][10] ILs the determined melting points were found to be in a good agreement with literature. However, for [C$_2$mim][SCN] there is a data discrepancy. Thus, the A.P. Abbott et al.[11] determined the melting point of [C$_2$mim][SCN] as -50 ^{o}C, while M. Forsyth et al.[12] showed the mp = -60 ^{o}C. Such difference in thermal properties can be explained by the choice of the synthetic method for IL. In A.P. Abbott et al.[11] work, the [C$_2$mim][SCN] was obtained by metathesis reaction between the chloride precursor and NH$_4$SCN. In contrast, M. Forsyth et al.[12] synthesized [C$_2$mim][SCN] by ion exchange between [C$_2$mim][I] and AgSCN. As [C$_2$mim][SCN] can dissolve silver thiocyanate to concentrations above 7 mol L^{-1} there is a possibility that in M. Forsyth's work,[12] [C$_2$mim][SCN] IL contained some amounts of AgSCN, thus leading to the formation of cocrystalls on cooling and subsequent change in melting process. The [C$_2$mim][SCN] used in this work was prepared by non-silver method and showed lower melting point of -56^{o}C (Figure S5), that is in a full agreement with that reported by A.P. Abbott et al.[11]

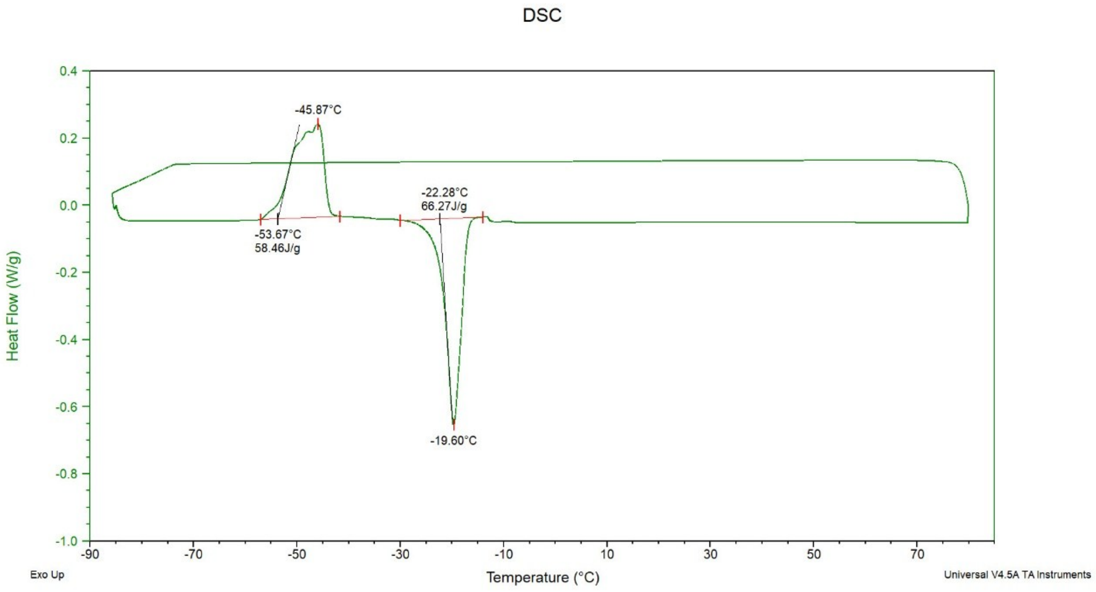

Figure S2. DSC curves for [C_2mim][TFSAM] at a heating rate of 2 °C min^{-1}.

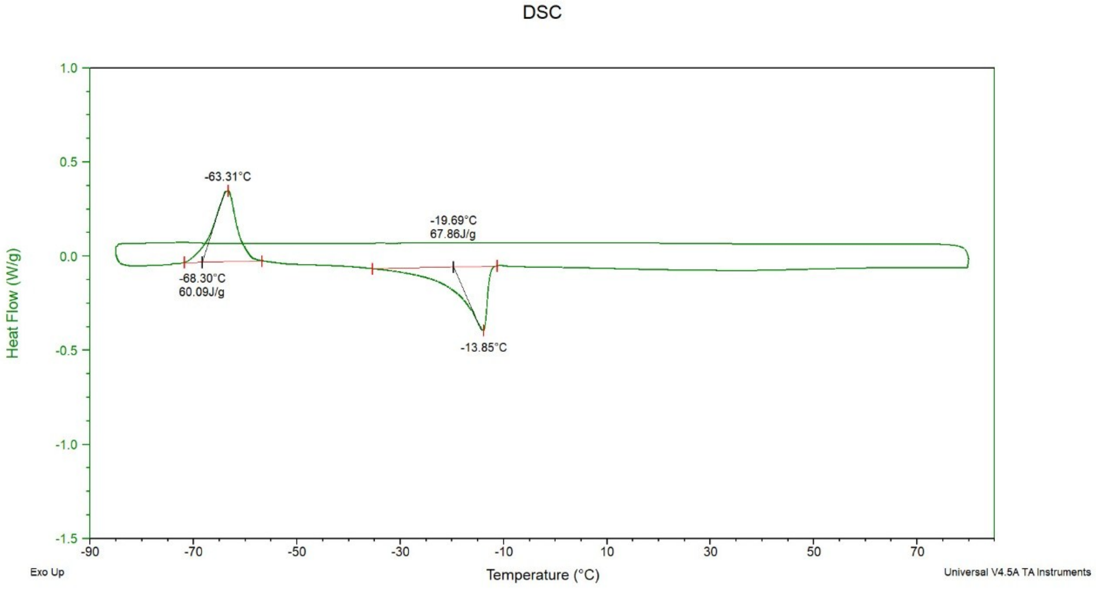

Figure S3. DSC curves for [C_2mim][$N(CN)_2$] at a heating rate of 2 °C min^{-1}.

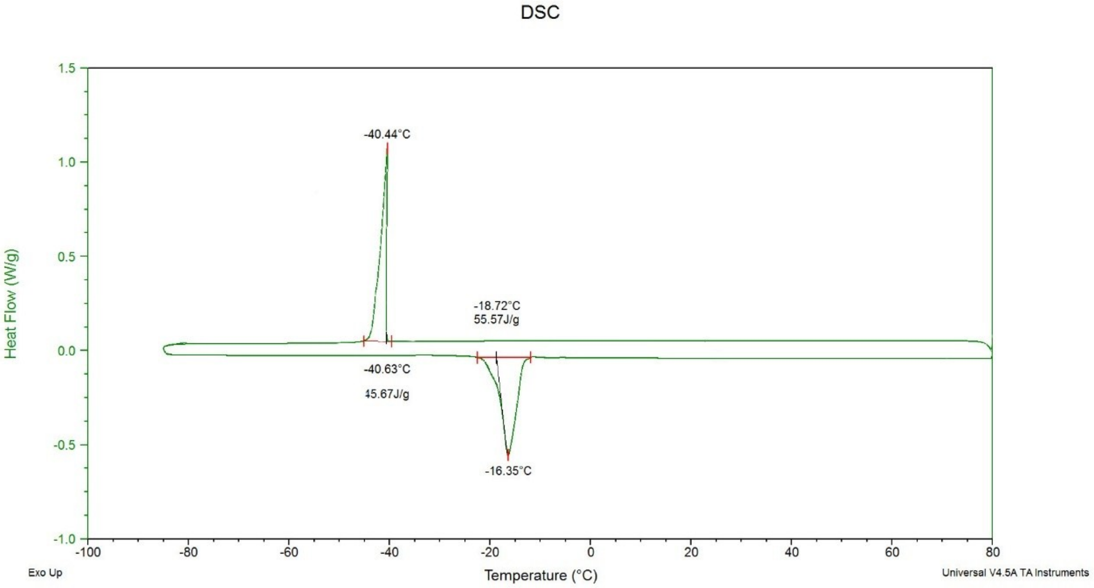

Figure S4. DSC curves for $[C_2mim][NTf_2]$ at a heating rate of 2 °C min^{-1}.

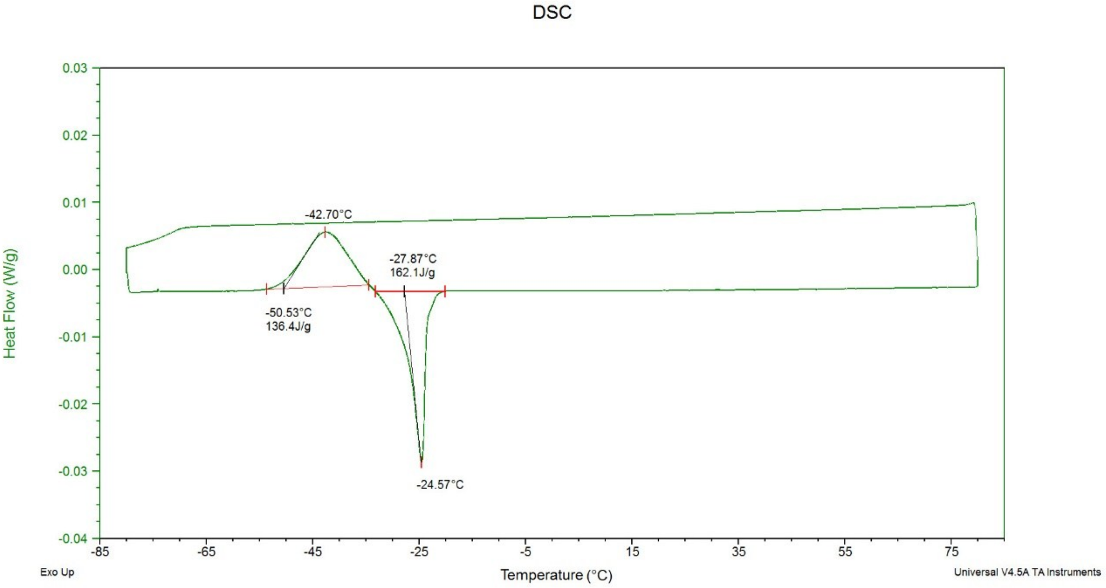

Figure S5. DSC curves for $[C_2mim][N(CN)_2]_{0.5}[NTf_2]_{0.5}$ mixture at a heating rate of 2 °C min^{-1}.

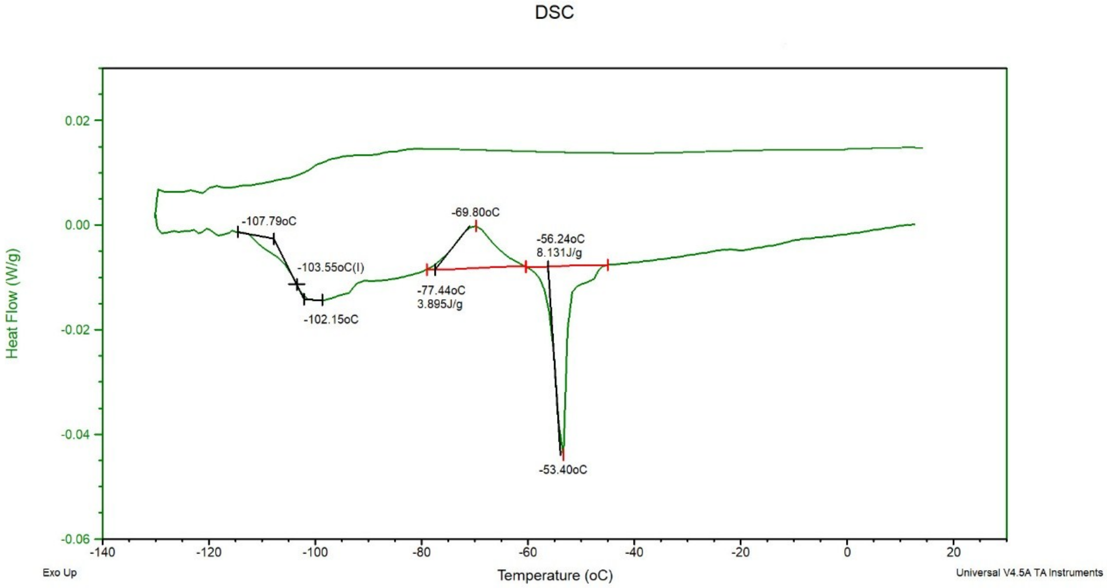

Figure S6. DSC curves for [C_2mim][SCN] at a heating rate of 2 °C min^{-1}.

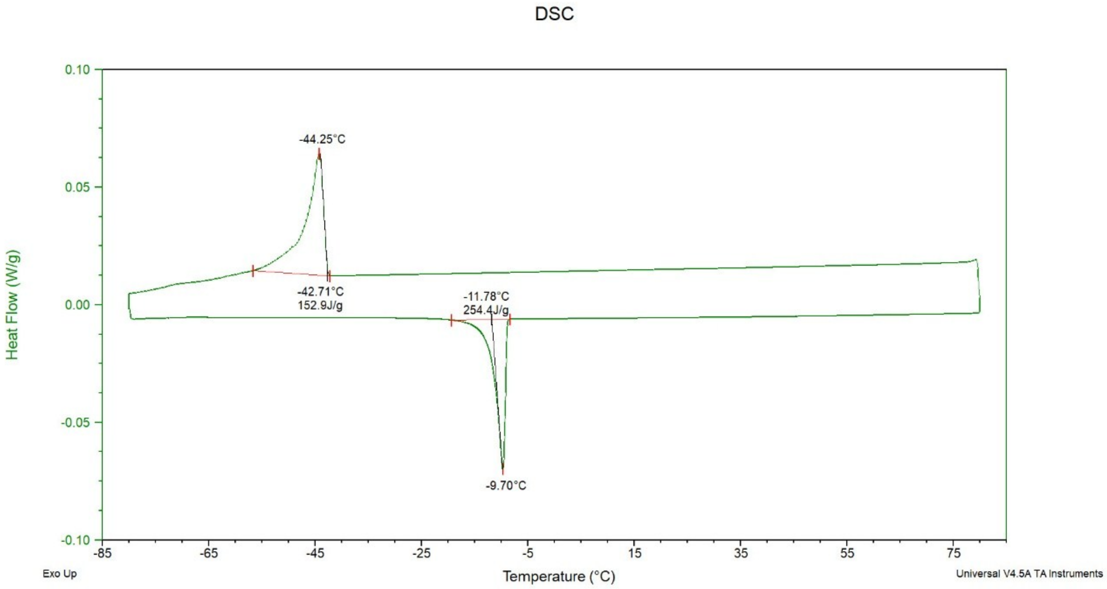

Figure S7. DSC curves for [C_2mim][CF_3SO_3] at a heating rate of 2 °C min^{-1}.

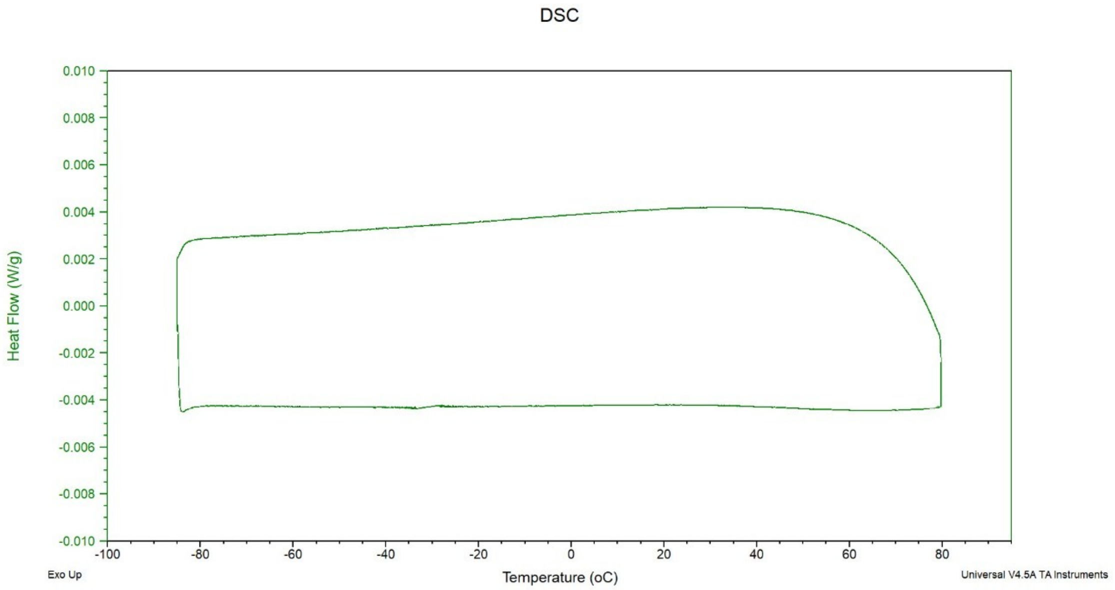

Figure S8. DSC curves for $[C_2mim][SCN]_{0.5}[CF_3SO_3]_{0.5}$ mixture at a heating rate of 2 °C min^{-1}.

Molecular Dynamics (MD) Simulation Details

All simulations were performed as previously described.[3] In brief, GROMACS 2016[13] was used for the simulation of 500 ion pairs of each ionic liquid or mixture. The CL&P force field[3, 14, 15] was selected to describe the inter- and intramolecular interactions of the molecules. The initial simulation boxes were prepared using Packmol[16] and the topology files build with DLPGEN 2.1.0.[17] The van der Waals and Coulomb interactions were considered to a distance of 1.6 nm, and the particle-mesh Ewald technique used to correct the electrostatic above this limit. The simulations were performed at 0.1 MPa and 300 K, by using a Parrinello-Rahman barostat (relaxation time of 5 ps; compressibility of 4.5×10^{-5}) and a v-rescale thermostat (relaxation time constant of 1 ps). The simulation boxes equilibration was achieved by performing several 5 ns runs. Once a constant density of the system was observed, a production run of 40 ns was made, collecting the trajectory each 100 ps for subsequent analysis. A timestep of 2 fs was used in all simulations. The analysis of the structure of the ionic liquids were performed by using the STRFACT package.[18, 19]

Total Structure Factor Functions Deconvolution

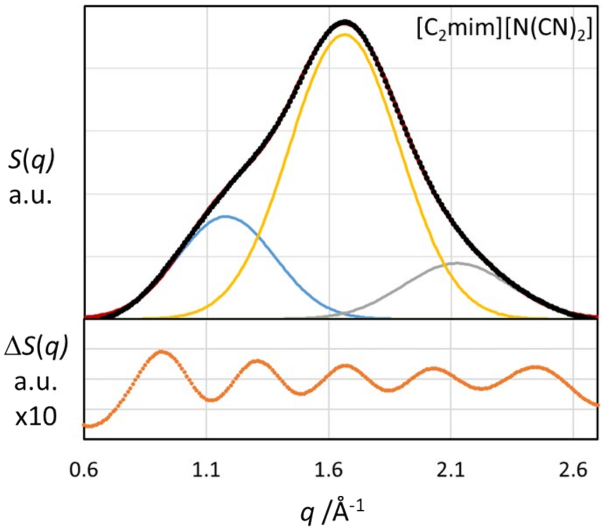

Figure S9. Deconvolution of the total structure factor function, $S(q)$, of the curve obtained for $[C_2mim][N(CN)_2]$. The black dots in the top representation are the data in Fig. 4 of the main text. The red line corresponds to the sum of the colored Gaussian functions in the figure, obtained from the fitting procedure. The representation in the bottom of the figure gives the fitting residues.

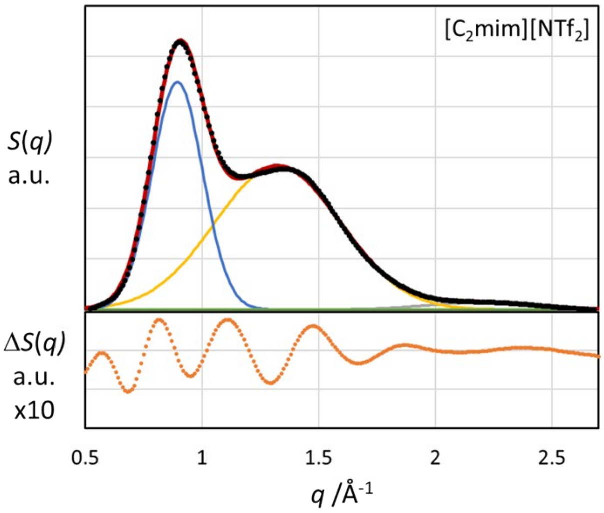

Figure S10. Deconvolution of the total structure factor function, $S(q)$, of the curve obtained for $[C_2mim][NTf_2]$. The black dots in the top representation are the data in Fig. 4 of the main text. The red line corresponds to the sum of the colored Gaussian functions in the figure, obtained from the fitting procedure. The representation in the bottom of the figure gives the fitting residues.

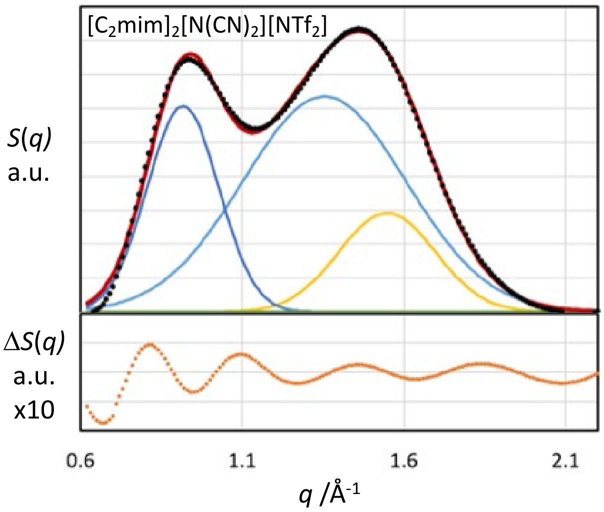

Figure S11. Deconvolution of the total structure factor function, *S*(*q*), of the curve obtained for $[C_2mim]_2[N(CN)_2][NTf_2]$. The black dots in the top representation are the data in Fig. 4 of the main text. The red line corresponds to the sum of the colored Gaussian functions in the figure, obtained from the fitting procedure. The representation in the bottom of the figure gives the fitting residues.

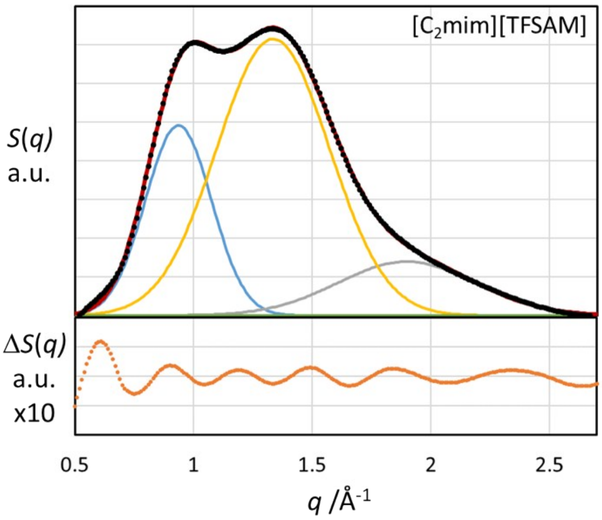

Figure S12. Deconvolution of the total structure factor function, *S*(*q*), of the curve obtained for $[C_2mim][TFSAM]$. The black dots in the top representation are the data in Fig. 4 of the main text. The red line corresponds to the sum of the colored Gaussian functions in the figure, obtained from the fitting procedure. The representation in the bottom of the figure gives the fitting residues.

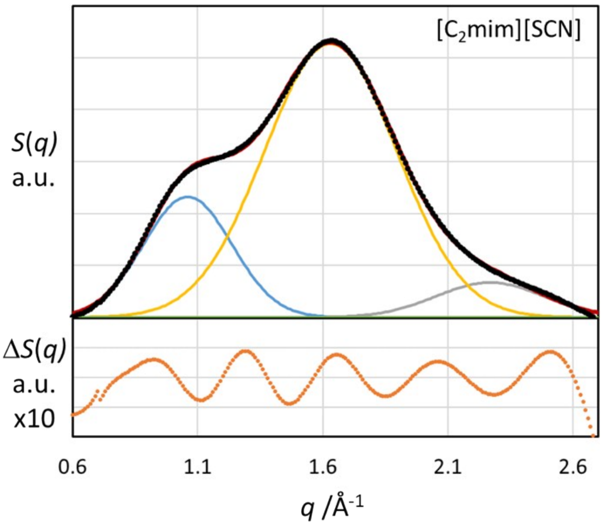

Figure S13. Deconvolution of the total structure factor function, *S*(*q*), of the curve obtained for [C_2mim][SCN]. The black dots in the top representation are the data in Fig. 4 of the main text. The red line corresponds to the sum of the colored Gaussian functions in the figure, obtained from the fitting procedure. The representation in the bottom of the figure gives the fitting residues.

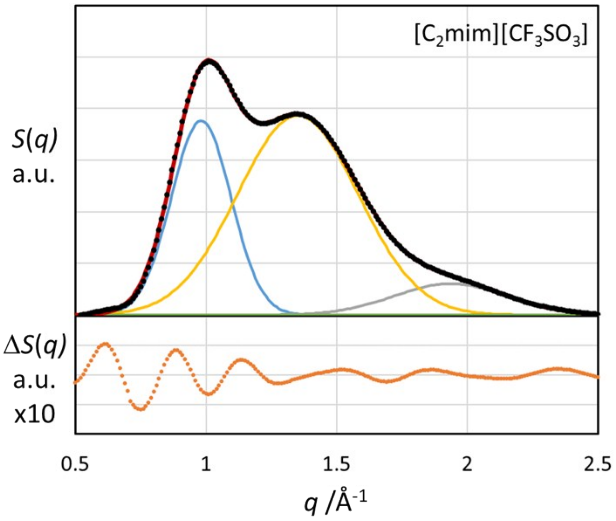

Figure S14. Deconvolution of the total structure factor function, *S*(*q*), of the curve obtained for [C_2mim][CF_3SO_3]. The black dots in the top representation are the data in Fig. 4 of the main text. The red line corresponds to the sum of the colored Gaussian functions in the figure, obtained from the fitting procedure. The representation in the bottom of the figure gives the fitting residues.

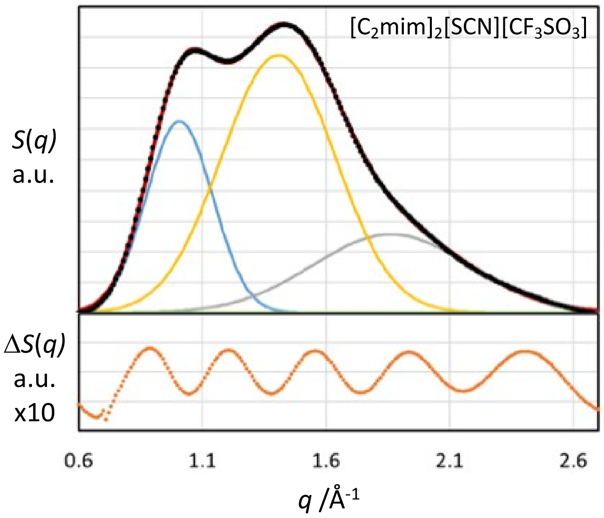

Figure S15. Deconvolution of the total structure factor function, *S*(*q*), of the curve obtained for [C_2mim][SCN][CF_3SO_3]. The black dots in the top representation are the data in Fig. 4 of the main text. The red line corresponds to the sum of the colored Gaussian functions in the figure, obtained from the fitting procedure. The representation in the bottom of the figure gives the fitting residues.

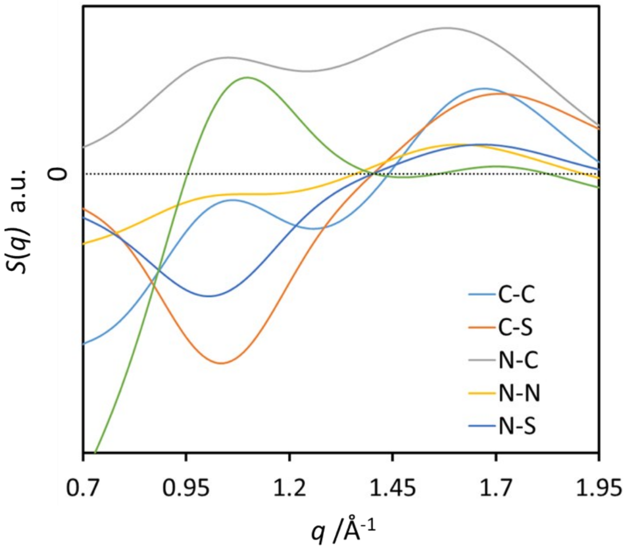

Figure S16. Deconvolution of the total structure factor function, S(q), of the curve obtained for [C_2mim][SCN], into the different atomic interactions contributions, as described in reference.[18] The dotted line represents the y = 0 line.

REFERENCES

1. A. S. Shaplov, E. I. Lozinskaya, P. S. Vlasov, S. M. Morozova, D. Y. Antonov, P. H. Aubert, M. Armand and Y. S. Vygodskii, *Electrochim. Acta*, 2015, **175**, 254-260.
2. A. S. L. Gouveia, L. C. Tome, E. I. Lozinskaya, A. S. Shaplov, Y. S. Vygodskii and I. M. Marrucho, *Phys. Chem. Chem. Phys.*, 2017, **19**, 28876-28884.
3. A. S. L. Gouveia, C. E. S. Bernardes, L. C. Tome, E. I. Lozinskaya, Y. S. Vygodskii, A. S. Shaplov, J. N. C. Lopes and I. M. Marrucho, *Phys. Chem. Chem. Phys.*, 2017, **19**, 29617-29624.
4. L. C. Tomé, D. J. S. Patinha, C. S. R. Freire, L. P. N. Rebelo and I. M. Marrucho, *RSC Adv.*, 2013, **3**, 12220-12229.
5. C. M. S. S. Neves, K. A. Kurnia, J. A. P. Coutinho, I. M. Marrucho, J. N. C. Lopes, M. G. Freire and L. P. N. Rebelo, *J. Phys. Chem. B*, 2013, **117**, 10271-10283.
6. L. Jin, K. M. Nairn, C. M. Forsyth, A. J. Seeber, D. R. MacFarlane, P. C. Howlett, M. Forsyth and J. M. Pringle, *J. Am. Chem. Soc.*, 2012, **134**, 9688-9697.
7. E. Gómez, N. Calvar and Á. Domínguez, 2015, DOI: 10.5772/59271, - Ch. 8.
8. D. R. MacFarlane, J. Golding, S. Forsyth, M. Forsyth and G. B. Deacon, *Chem. Commun.*, 2001, DOI: 10.1039/B103064G, 1430-1431.
9. S. V. Dzyuba and R. A. Bartsch, *ChemPhysChem*, 2002, **3**, 161-166.
10. P. Bonhôte, A.-P. Dias, N. Papageorgiou, K. Kalyanasundaram and M. Grätzel, *Inorg. Chem.*, 1996, **35**, 1168-1178.
11. A. P. Abbott, E. I. Ahmed, R. C. Harris and K. S. Ryder, *Green Chem.*, 2014, **16**, 4156-4161.
12. J. M. Pringle, J. Golding, C. M. Forsyth, G. B. Deacon, M. Forsyth and D. R. MacFarlane, *J. Mat. Chem.*, 2002, **12**, 3475-3480.
13. M. J. Abraham, T. Murtola, R. Schulz, S. Páll, J. C. Smith, B. Hess and E. Lindahl, *SoftwareX*, 2015, **1-2**, 19-25.
14. J. N. Canongia Lopes, J. Deschamps and A. A. H. Pádua, *J. Phys. Chem. B*, 2004, **108**, 2038-2047.
15. J. N. Canongia Lopes and A. A. H. Pádua, *Theor. Chem. Acc.*, 2012, **131**, 1129.
16. M. L., A. R., B. E. G. and M. J. M., *J. Comput. Chem.*, 2009, **30**, 2157-2164.
17. C. E. S. Bernardes and A. Joseph, *J. Phys. Chem. AJ. Phys. Chem. A*, 2015, **119**, 3023-3034.
18. C. E. S. Bernardes, K. Shimizu and J. N. Canongia Lopes, *Mol. Simul.*, 2018, **44**, 478-484.
19. K. Shimizu, C. E. S. Bernardes, A. Triolo and J. N. Canongia Lopes, *Phys. Chem. Chem. Phys.*, 2013, **15**, 16256-16262.